Observational constraints on the evolution of dust in protoplanetary disks

Martins e Oliveira, I.

3

Spectroscopic properties of Young Stellar Objects in the Lupus Molecular Clouds

The results of an optical spectroscopic survey of a sample of young stellar objects (YSOs) and pre-main sequence (PMS) stars in the Lupus Clouds are presented. 92 objects were observed with VLT/FLAMES. All of those objects show IR excess as discovered by the *Spitzer* Legacy Program "From Molecular Cores to Planet-Forming Disks" (c2d). After reduction, 54 spectra with good signal-to-noise ratio are spectrally classified. Effective temperatures and luminosities are derived for these objects, and used to construct H-R diagrams for the population. The sample consists mostly of M-type stars, with 10% K-type stars. Individual ages and masses are inferred for the objects according to theoretical evolutionary models. The mean population age is found to be between 3.6 and 4.4 Myr, depending on the model, while the mean mass is found to be $\sim$0.3 $M_{\odot}$ for either model. Together with literature data, the distribution of spectral types is found to be similar to that in Chamaeleon I and IC348. The Hα line in emission, found in 49% of the sample, is used to distinguish between classical and weak-line T Tauri stars. 56% of the objects show Hα in emission and are accreting T Tauri stars. Mass accretion rates between 10^{-8} and 10^{-11} $M_{\odot}$ yr^{-1} are determined from the full width at 10% of the Hα peak intensity.

Annelies Mortier, Isa Oliveira and Ewine F. van Dishoeck
Submitted to Monthly Notices of the Royal Astronomical Society

3.1 Introduction

Lupus Molecular Clouds is the generic denomination of a loosely connected concentration of dark clouds and low-mass pre-main sequence stars located in the Scorpius-Centaurus OB association at $16^h20^m < \alpha < 15^h30^m$ and $-43° < \delta < -33°$. Due to its large size, close distance (d = 150–200 pc) and substantial mass of molecular gas, the Lupus Clouds have been subject of many studies at all wavelengths over the years (e.g. Hughes et al. 1994; Merín et al. 2008; see Comerón 2008 for a review; Comerón et al. 2009; Tothill et al. 2009).

Lupus is one of the five clouds selected by the *Spitzer* Legacy Program *"From Molecular Cores to Planet-Forming Disks"*, also referred to as c2d (Cores to Disks, Evans et al. 2003). Using 400 hours of observations and all three instruments of *Spitzer*, the c2d program studies the process of star and planet formation from the earliest stages of molecular cores to the epoch of planet-forming disks. The five observed clouds cover a range of cloud types broad enough to study all modes of low-mass star formation, and large enough to allow statistical conclusions. A rich population of low-mass young stellar objects (YSOs) still surrounded by their circumstellar material has been discovered by *Spitzer* in these clouds (Harvey et al. 2007a,b; Merín et al. 2008; Evans et al. 2009).

Disks around YSOs, called protoplanetary disks, consist mainly of dust and gas. Dust particles of sub-μm size dominate the disk opacity, making it easily observable at infrared and (sub-)millimeter wavelengths by re-emitting some of the received stellar radiation. Dust emission is also temperature dependent with colder dust emitting at longer wavelengths than warm dust. Protoplanetary disks evolve in time, ending up in different scenarios like a planetary system or a debris disk, that may or may not also harbor planets.

The stellar radiation spectrum depends on the effective temperature of the star. Because of the properties of dust emission, the IR excess in a spectral energy distribution (SED) of this star+disk system provides information about the geometry and properties of the dusty disk. To separate star and disk emission, the stellar characteristics need to be known. The inner regions of the circumstellar disk are disrupted by the stellar magnetosphere. The stellar magnetic field creates channels through which material can flow from the disk onto the star. This produces atomic lines from hydrogen, calcium, oxygen, etc. The strongest emission line is Hα at 6562.8 Å.

The Lupus complex is one of the largest low-mass star forming regions on the sky, with four main star forming sites, referred to as Lupus I-II-III-IV. Furthermore, Lupus III contains one of the richest associations of T Tauri stars (see Comerón 2008 for a review). The work presented here concentrates on data from Lupus I, III and IV because those were the regions observed by the c2d program. Their star formation rates are 4.3, 31 and 4.5 $M_\odot$ Myr^{-1}, respectively (Evans et al. 2009). Distances of 150 ± 20 pc for Lupus I and IV and 200 ± 20 pc for Lupus III are assumed in this work (Comerón 2008).

We present an optical spectroscopic survey designed to characterize the young

stellar population of Lupus I, III and IV, as observed by the c2d program. Section 3.2 describes the selection criteria for the sample and Section 3.3 the observations and data reduction. Using libraries of standards from the literature, spectral types and effective temperatures are obtained in Section 3.4. Combined with additional photometric data, the SEDs of the objects can be built. In Section 3.5, the stellar and disk luminosities are calculated from the SEDs. In Section 3.6, the stars are placed in Hertzsprung-Russell diagrams and individual masses and ages are derived based on theoretical tracks. The mass accretion rates, determined through the Hα line, are presented in Section 3.7. In Section 3.8 the young stellar population of Lupus is discussed in context with other regions. Finally, in Section 3.9, the conclusions from this work are stated.

3.2 Sample Selection

Merín et al. (2008) used the *Spitzer* c2d point source catalog to identify the YSO population in the Lupus clouds. Objects are classified as YSO if they show an IR excess in the SED. To obtain an optimal separation between young stars, background galaxies and Galactic post-AGB stars, Merín et al. (2008) used the selection criteria developed by the c2d team on its official point source catalog (Evans et al. 2007). The method relies on an empirical probability function that depends on the relative position of any given source in several color-color and color-magnitude diagrams where diffuse boundaries have been determined.

The list of YSOs from Evans et al. (2007) was then adapted by Merín et al. (2008). Visual inspection was performed to subtract suspected galaxies or binaries, leaving the list with 94 YSOs. The final list of Merín et al. (2008) was merged with 65 pre-main sequence (PMS) stars and PMS candidates. Here, the term PMS star is used for other objects added to the list whose youth had already been confirmed using other observational techniques, mainly optical spectroscopy. If an object has not been spectroscopically confirmed as young but it was selected by its optical and near-IR photometry as such, it is labeled as a PMS candidate. This final list of 159 young objects is used for the observations presented here.

3.3 Observations and Data Reduction

The data presented here were taken in the second half of the nights of 20 – 25 February 2008 with the Very Large Telescope (VLT) and the instrument FLAMES/GIRAFFE (ID: 080C.0473-A, PI: Oliveira). The instrument was used in the MEDUSA mode, with wavelength coverage of 6437 – 7183 Å, and spectral resolution of 0.2 Å. This wavelength range was chosen for containing temperature sensitive features, useful for spectral classification. Additionally, it covers the Hα line, an accretion diagnostic. MEDUSA has 135 fibers available, each with an aperture of 1.2″. In total, 250 stars in 19 fields were observed (on average: 14 stars per field). Of those, 158 are field stars, leaving the Lupus science sample with 92 objects. An overview of the observations

can be found in Table 3.1. The different exposure times are adjusted to the mean magnitude of the objects in a given field to avoid saturation of the brightest sources.

The VLT data pipeline, GASGANO, was used for the data reduction. For each observation night, a set of 5 dark frames, 3 flat-fields and 1 arc frame are produced. GASGANO performs bias subtraction, flat-fielding and wavelength calibration. Further spectral extraction was performed within IDL. In each observed field, unused fibers were placed in random "empty" sky positions. Those positions are not really "empty" sky, since the cloud itself can contribute to the sky with a lot of emission lines. In each field, all the sky spectra are combined within IDL into one master sky spectrum, with a 2σ clipping. This combined sky is then subtracted from the science spectra to obtain spectra that are ready for analysis.

The spectra are sorted into four categories: good spectra, non-detection with a mean flux around zero, featureless spectra and not useful spectra (marked as G, U, F and O respectively in Table 3.1). The two spectra classified as not useful for our science purpose are objects # 14 and 53. Object 14 was discovered to be a galaxy (see section 3.4.2) while object 53 was observed with a broken fibre, resulting in an unclassifiable spectrum. The non-detections (marked 'U', 23 objects) and featureless (marked 'F', 13 objects) spectra could also not be spectrally classified. This leads to 54 good classifiable spectra, out of which 27 have very good signal-to-noise ratio.

3.4 Spectral Classification

3.4.1 Method

From the obtained spectra, the YSOs were classified by comparing their spectral features with libraries of standard stars. To match the high resolution of the FLAMES spectra, high resolution standards from Montes (1998) were used. However, standards for all spectral types are not available in this library, so that only a range of spectral types can be derived from it. To further the analysis and narrow down the spectral type, a low resolution (3.58 Å) library was used as well (G. Herczeg, private communication, 2010). Once a spectral type range has been determined from the high resolution standards, the low resolution library is used for a finer determination due to the availability of standards of nearly all spectral types in this library.

The most prominent features in late type stars are the Titanium Oxide (TiO) absorption lines at 7050 – 7150 Å. Mostly K-type and M-type stars have these features because they are cold enough for TiO to exist. The TiO feature at these wavelengths shows three absorption bands, which are deeper for colder objects. The Li I line in absorption at 6707 Å is also a common feature in young stars. This line could, however, not be clearly detected in these objects, due to the often low signal-to-noise ratio and limited spectral resolution.

To compare with the high resolution standards, the science spectra are normalized (divided by the continuum) and overplotted on the normalized standard spectra of different spectral types (see Figure 3.1). A spectral range is visually determined by

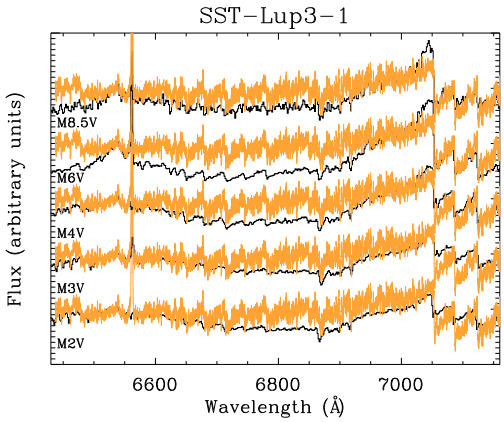

Figure 3.1 – Example of the classification method of SST-Lup3-1 with high resolution standards. The black curves represent the high resolution standard models and the gray curves the science spectrum. At the left of each standard its spectral type is indicated. The range of plausible spectral types is determined to be M4 - M8.5

the best match for the TiO bands. The method for the low resolution standards is somewhat different because that library is not normalized. First, the resolution of the science spectra is lowered to that of the standard (3.59Å). This is done by convolving the spectrum with a Gaussian profile. The comparison of the spectra with the low resolution standards then happens in two ways. One way consists of scaling the spectra to the standards by anchoring their fluxes at certain wavelengths (6500, 7020 and 7050 Å). An example is shown in Figure 3.2 (top left, top right and bottom left). In the alternative method a scale factor is determined by first dividing both spectra and then taking the mean of those values, ignoring extreme features (like Hα emission lines) in the process. This factor is then used to scale the original spectra to the standards (see bottom right panel of Figure 3.2). Both methods agree very well, producing four different plots for each spectral type within the determined range. The correct spectral type is again visually determined by the best match at the TiO bands. The typical uncertainty in the spectral classification is one sub-class.

3.4.2 Special Spectra

Some spectra present special features besides the temperature sensitive ones used for spectral classification. These objects were inspected more closely and are differentiated in three special types of spectra:

- Ten spectra show [He I] emission lines at 6677.6 and 7064.6 Å (objects # 7, 52, 76, 82, 83, 84, 85, 87, 91, 93 - see examples in Figure 3.3). All of these objects also show strong Hα in emission. Strongly accreting objects produce emission lines other than Hα, such as this line. It is concluded that these lines are a sign

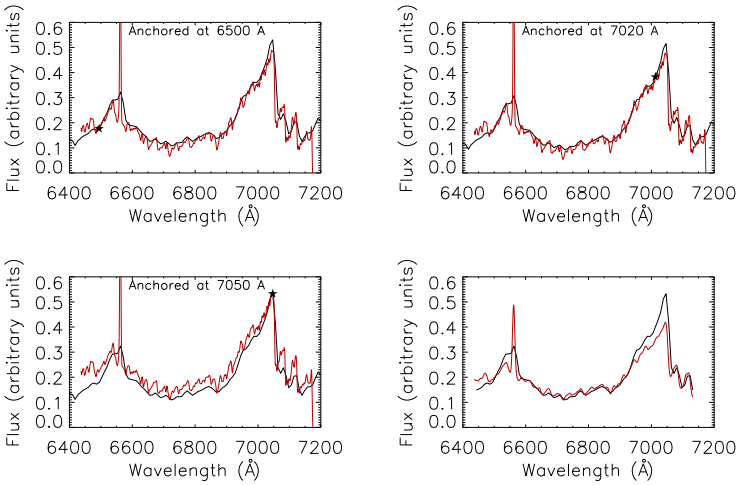

Figure 3.2 – Example of the classification methods of SST-Lup3-1 with the low resolution standard of a M6 main sequence star. The first three panels show the first method where the spectra are anchored at different wavelengths (wavelength explicitly mentioned in each plot, and marked to guide the eye). The last panel shows the second method. In all plots, the model is shown in black and the science spectrum in gray.

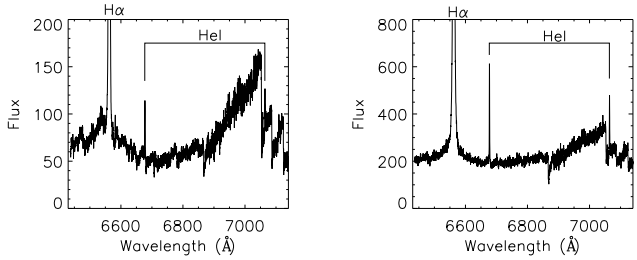

Figure 3.3 – Sample of spectra (#82 on left panel and #7 on right panel) with strong Hα (6562.8 Å), and He I (6677.6 and 7064.6 Å) emission lines.

of accretion, as is Hα (see Section 3.7 for more information on this subject).

- Four spectra (objects #50, 59, 78 and 88) show the [NII] doublet at 6548.4 and 6583.4 Å and the [SII] doublet at 6715.8 and 6729.8 Å (see examples in Figure 3.4). These lines are indicative of ionised gas. Par-Lup3-4 (#50) and Sz102 (#78) are related to Herbig-Haro (HH) objects HH600 and HH228 respectively (Wang & Henning 2009). They classified these objects to be HHs with the [SII] doublet line at 6717/6731 Å. The two other objects that show similar spectra, SSTc2dJ160708.6-391407 (#59) and Sz133 (#88), are not yet classified

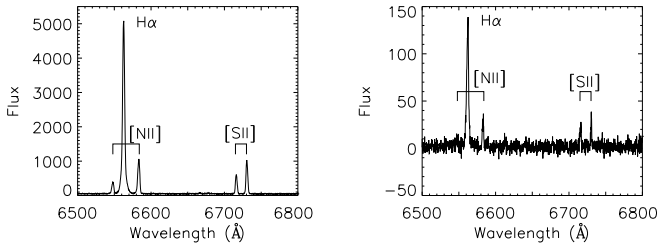

Figure 3.4 – Sample of spectra (#78 on left panel and #59 on right panel) with [NII] and [SII] doublets (at 6548.4 and 6583.4, and 6715.8 and 6729.8 Å respectively). Those sources may be associated with Herbig-Haro objects.

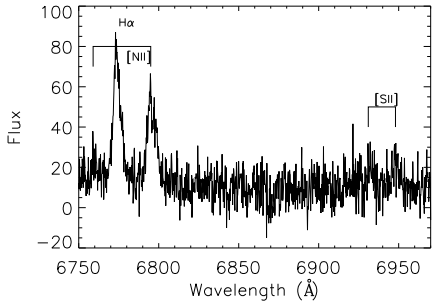

Figure 3.5 – Spectrum of IRAS15589-4132. The emission lines correspond with the spectral lines [N II] (at 6548.4 and 6583.4 Å) and [S II] (at 6715.8 and 6729.8 Å). This object is identified as a galaxy at redshift $z = 0.0324$.

as Herbig-Haro, and are thus designated as Herbig-Haro candidates.

- One spectrum, IRAS15589-4132 (#14), shows lines at 6757.95, 6774, 6794.8, 6931.5 and 6947.8 Å, and no other features (see Figure 3.5). These lines are identified as the doublets [N II] (at 6548.4 and 6583.4 Å) and [S II] (at 6715.8 and 6729.8 Å) and the strongest Hα line (at 6562.8 Å) at a redshift $z = 0.032$. This suggests that the object is a red-shifted galaxy rather than a YSO in the Lupus Cloud. In the NASA/IPAC Extragalactic Database (NED), there is a galaxy classified at the position of this object: 2MASSJ16022165-4140536. For further analysis, this object will no longer be considered part of the sample, leaving 91 sources in total.

3.4.3 Spectral Types

Following the method described above, the resulting spectral types with their error ranges are listed in Table 3.2. The objects are mostly M-type stars, but 10% are

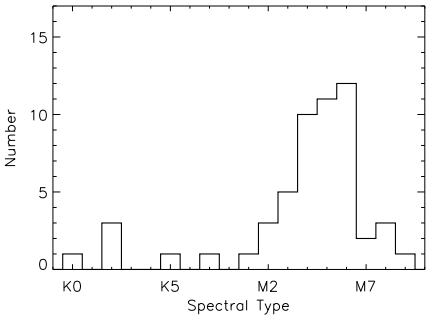

Figure 3.6 – Distribution of spectral types found in this work. The distribution peaks at M4–M6.

K-type. The histogram in Figure 3.6 shows the spectral type distribution, peaking at M6.

40 of these 54 objects were designated by Merín et al. (2008) as YSOs. Spectral classification is found in the literature for 31 of the 54 objects (57%). The literature classifications match well (within one sub-class) with those derived here. One object, however, differs: object # 26 is classified by López Martí et al. (2005) as M5, but as K0 (range from K0 to K2) here. For further analysis, our derived values are used.

3.4.4 Effective Temperature

Because spectral types are directly related to effective temperature T_{eff}, the temperatures of the stars classified here can be obtained (see Table 3.3). For spectral types in the range K – M0, the relationship adopted by Kenyon & Hartmann (1995) was used, while the relationship from Luhman et al. (2003) was adopted for types later than M0. The uncertainties in the temperature are determined directly from the spectral type uncertainties.

3.5 Spectral Energy Distributions

For a given star with known spectral type (and therefore T_{eff}), an SED can be constructed using the correct stellar atmosphere model and additional photometric data. The templates for stellar atmospheres used here are the NextGen Model Atmospheres (Hauschildt et al. 1999; Allard et al. 2000). In addition, various photometric datasets are available for the objects in Lupus. Optical and near-IR photometry in the R_C, I_C and Z_{WFI} bands (at 0.6517, 0.7838 and 0.9648 μm, respectively) was obtained from Comerón et al. (2010, private communication). The data were taken with the Wide Field Imager (WFI) at the La Silla 2.2 m Telescope in Chile. Near-infrared Two Micron All-Sky Survey (2MASS) photometry at J, H and K (at 1.235, 1.662 and 2.159 μm, respectively) is publicly available. Finally, *Spitzer* mid-infrared data at the

IRAC and MIPS bands (at 3.6, 4.5, 5.8, 8.0, 24 and 70 μm, respectively) are also available online [1] (Evans et al. 2003).

For each object, its photometric data and corresponding NextGen model atmosphere are used (matching its spectral type and the gravitational acceleration for a pre-main-sequence star). The observed photometric data are corrected for extinction at all wavelengths from the object's visual extinction (A_V), using the extinction law by Weingartner & Draine (2001) with $R_V = 5.5$. Subsequently, the NextGen atmosphere is scaled to the extinction corrected photometric data at a given band. The scaling band used is either the $z_{\rm WFI}$ or J band, depending on the availability of the photometry and the quality of the fit. In Table 3.2, the extinction values and normalization bands are presented for all fitted objects.

Figure 3.7 shows the constructed SEDs for 41 out of 54 objects. Here, the solid black line is the NextGen model atmosphere, the open squares are the observed photometry while filled circles show the extinction corrected data. SEDs could not be produced for 13 out of the 54 spectrally classified objects. Either not enough infrared (both 2MASS as Spitzer) photometry is available, or the different photometric data (optical, 2MASS and Spitzer) did not match well with each other.

A wide variety of SEDs can be seen in Figure 3.7. Consequently, a wide variety in disk types is inferred. The infrared spectral index slope can be used as a characteristic to distinguish between Class I, II and III objects, as defined by Lada. For the 39 objects with available data in K and MIPS1, the slope can be calculated as:

$$\alpha_{2-24\mu m} = \frac{(\lambda F_\lambda)_{24\mu m} - (\lambda F_\lambda)_{2\mu m}}{\lambda_{24\mu m} - \lambda_{2\mu m}}$$

These values are shown in Table 3.2. One object has $\alpha_{2-24\mu m}$ consistent with a Class I source ($\alpha > 0$) and 15 consistent with Class III sources ($\alpha < -2$), the majority of them are Class II, disk sources. Additionally, object #67 is a confirmed cold disk, as studied by Merín et al. (2010). Cold disks are disks with large inner dust holes (i.e. lack of warm dust). Objects # 27, 79 and 80 have SEDs consistent with inner dust holes. Although confirmation of their nature as cold disks requires SED modelling that is out of the scope of this work, 4 out of 41 objects with SEDs in Figure 3.7 amount to ∼10% of cold disks in the sample, which is consistent with the range of 4 – 12% of cold disk frequency derived by Merín et al. (2010).

3.5.1 Luminosities

Stellar and disk luminosities can be derived for the objects for which SEDs could be plotted. Stellar luminosity is calculated with the formula:

$$L_* = 4\pi D^2 \int F_\lambda d\lambda$$

[1] htpp://ssc.spitzer.caltech.edu/spitzerdataarchives/

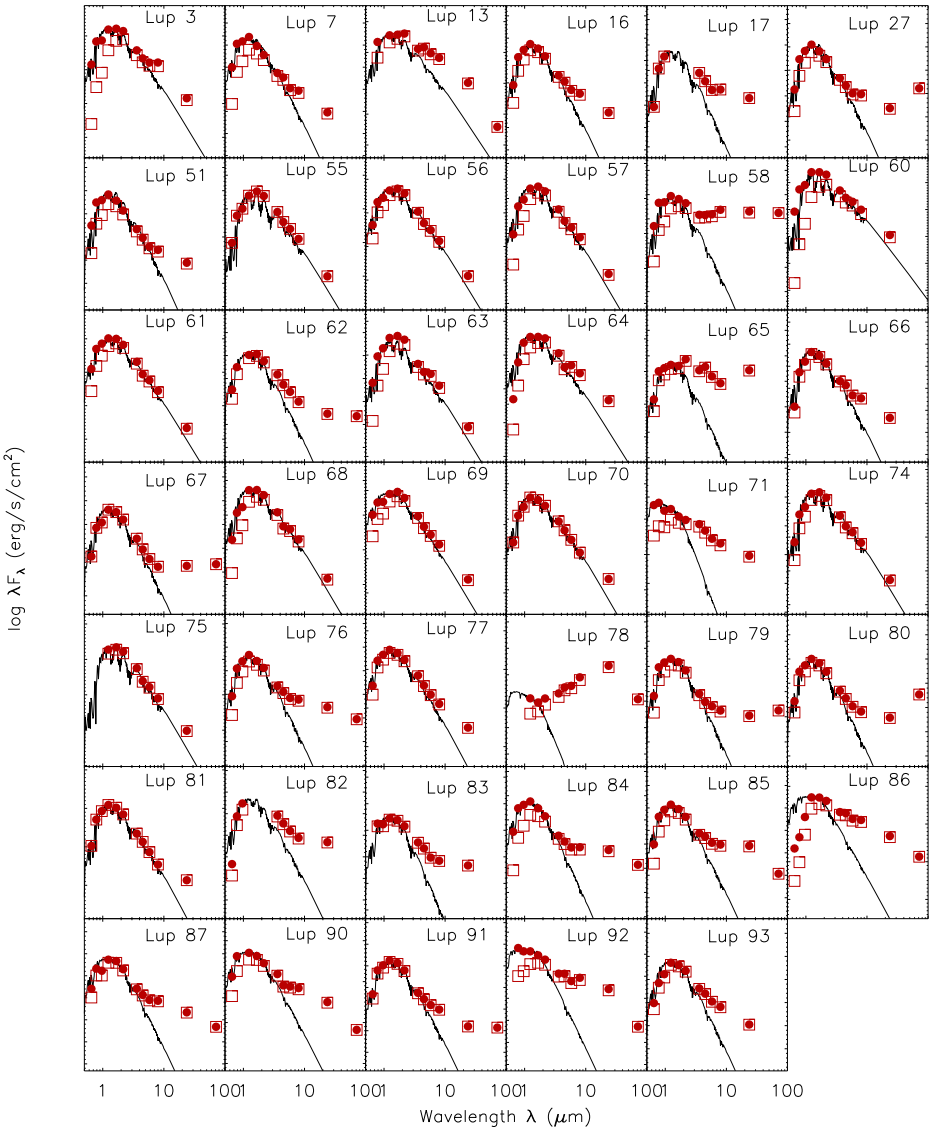

Figure 3.7 – SEDs of all the objects. The thick black curve is the model atmosphere of a star at its given temperature. The open points are the observed optical, 2MASS and *Spitzer* data. The closed points are the extinction corrected data. Notice the wide variety in SEDs (and thus disk shapes).

where D is the distance to the source and F_λ is the stellar flux – an integration of the NextGen model atmosphere scaled and normalized to the dereddened photometric data. Errors are derived from the uncertainty in the distance and flux, which includes an error in A_V of ± 0.5 mag. The disk luminosity is the integrated excess emission above the stellar photosphere. Errors are derived from the stellar luminosity errors. Those two values are shown in Table 3.3.

3.6 H-R Diagram

The age and mass of a star can be derived from theoretical tracks, overlaid on physical H-R diagrams. The position of an object in the H-R diagram is determined by its temperature (derived in Section 3.4.4) and luminosity (derived in Section 3.5.1).

3.6.1 Results

The pre-main sequence evolutionary tracks of Baraffe et al. (1998, 2001) and Siess et al. (2000) are overlaid in the H-R diagrams where the objects in this sample are placed (Figure 3.8). Thirteen objects are outside the range of the tracks (red and yellow circles in Figure 3.8).

Three objects (marked in red) are below the tracks: ID # 65, 71 and 78. By looking at their SEDs in Figure 3.7, it can be seen that objects 65 and 78 have substantial IR excess. The stellar fluxes are also not that high. These may be objects still surrounded by envelopes, which could be responsible for their low luminosity. Another explanation is that the objects are seen edge-on, such that the dust in the disk blocks some of the light of the star. In both cases, the calculated luminosity will be too low, resulting in an incorrect placement in the HR diagram. Object 71 does not to have a lot of IR excess. The reason of its misplacement in the HR diagram could be that it is a background source and is in fact at a larger distance, which will increase the calculated luminosity.

Ten objects (marked in yellow) are above the tracks: ID 3, 13, 55, 60, 61, 63, 64, 68, 74 and 75. An easy explanation would be that the assumed distance is wrong and that the objects are actually closer to us. However, even with very small distances (e.g. 60 pc), the objects are still above the tracks. Other effects have to play a role. One option is that they are part of a binary system that is unresolved, resulting in a stellar luminosity that is too high. Another option is that they are evolved AGB-stars. The working assumption is that these objects, however, do not belong to the Lupus Clouds.

For those 13 objects, no ages and masses were derived. For the other objects, the effective temperature, stellar and disk luminosity, age and mass can be found Table 3.3. As can be seen from Figure 3.9, the two models agree on the range of ages and masses, albeit with a different distribution. The mean age is 3.6 Myr for the Baraffe models and 4.4 Myr for the Siess models. For the masses, both models determine a mean stellar mass of only 0.3 $M_\odot$. This result is in agreement with that derived

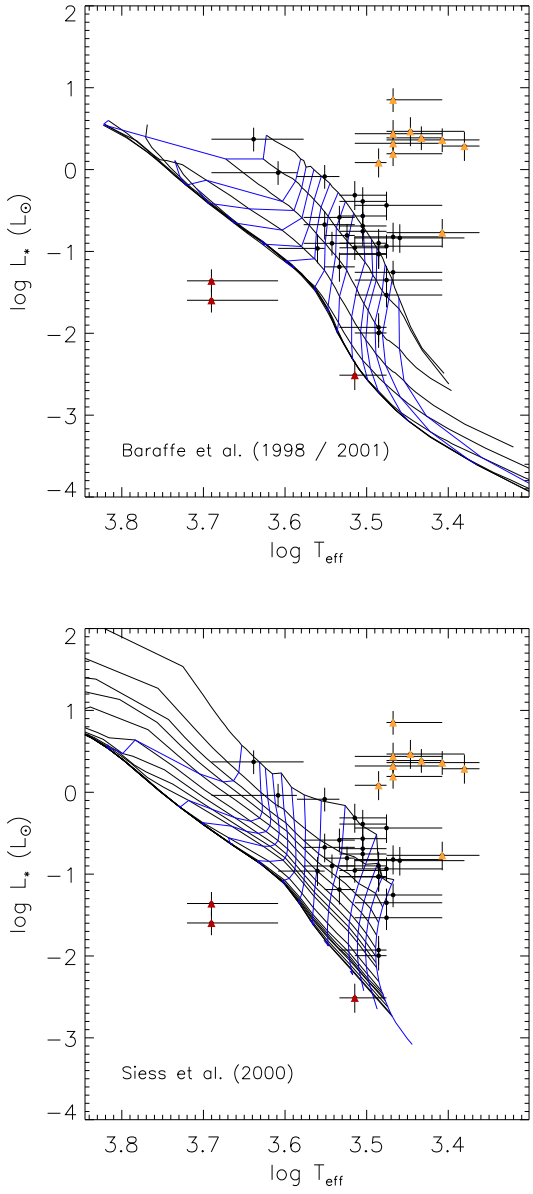

Figure 3.8 – HR diagram of the objects. Overlaid are the isochrones (black) and mass tracks (gray). The top panel shows the tracks from Baraffe et al. (1998, 2001) and the bottom panel the tracks from Siess et al. (2000). The corresponding ages (in Myr) and masses (in $M_\odot$) are marked. The red and yellow circles are objects that do not follow the tracks.

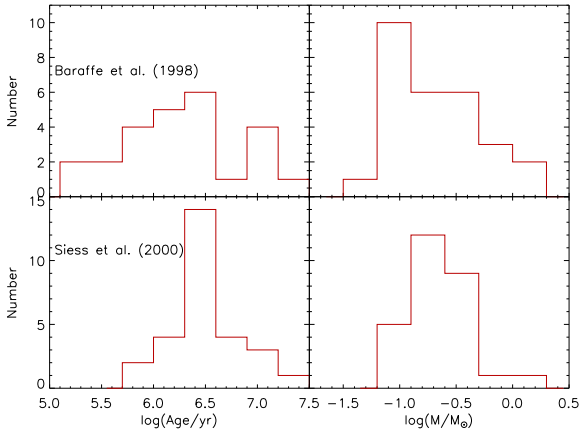

Figure 3.9 – Histograms of the ages and masses as derived from the two models.

by Merín et al. (2008). When deriving a luminosity function for the young stellar population in Lupus, the authors found it to peak at 0.2 $L_\odot$, which corresponds to 0.2 $M_\odot$ according to the PMS evolutionary tracks of Baraffe et al. (1998).

3.7 Accretion Based on Hα in Emission

From the data presented here, 45 of the objects (48 %) show the Hα line in emission. The strength of the Hα emission line is often used to distinguish between two classes of pre-MS stars: classical T Tauri stars (CTTS) and weak-line T Tauri stars (WTTS). CTTS are believed to correspond to stars that are actively accreting and WTTS are not, respectively. To this end, different methods have been proposed in the literature. Here, two methods are explored: the equivalent width and the full width of Hα at 10% of its peak intensity.

3.7.1 Hα Equivalent Width

The value of equivalent width (EW) can be used to distinguish between accreting and non-accreting objects, with the dividing threshold depending on the spectral type of the star. White & Basri (2003) proposed that a star is a CTTS if EW[Hα] $\geq$ 3 Å for K0–K5 stars, EW[Hα] $\geq$ 10 Å for K7–M2.5 stars, EW[Hα] $\geq$ 20 Å for M3–M5.5 stars and EW[Hα] $\geq$ 40 Å for M6–M7.5 stars. It is important to note that stars with EW[Hα] values lower than these proposed levels are not necessarily WTTS. Extra confirmation is needed from other diagnostics such as the Lithium abundance.

Following this criterion, 24 of the 45 objects (53.3%) are considered to be actively accreting (values can be found in Table 3.4). For objects # 22, 49, 50 and 59, no spectral type is available. However, since the EWs of these 4 objects are greater than 40 Å, they are considered accreters anyway.

3.7.2 Full Width of Hα at 10% of Peak Intensity

White & Basri (2003) proposed the use of another quantity to distinguish accreting and non-accreting objects: the full width of the line at 10% of the peak intensity, Hα[10%]. Lines with Hα[10%] > 270 km s^{-1} are, according to their measurements, assumed to be accreting. Based on physical reasoning as well as empirical findings, Jayawardhana et al. (2003) adopted 200 km s^{-1} as a more reasonable accretion cut-off, especially for low-mass stars. This is the cut-off value used in this work.

By performing a Gaussian fit (see Figure 3.10), Hα[10%] values can be obtained. To account for the resolution, the measured FWHM of each profile must be deconvolved assuming a Gaussian instrumental profile. For this sample, the Hα[10%] values can be found in Table 3.4. The errors are propagated from the error in the Gaussian fit to the error on the spectral resolution. According to the criterion of Jayawardhana et al. (2003), 25 of the 45 objects (55.5%) are considered accreters. The other 20 objects are not consistent with CTTS, even within their uncertainties. They are classified as non-accreters.

Some line profiles show broad wings at the bottom, which cannot be properly fitted by a Gaussian. In order to reproduce those lines, Voigt profiles were fitted to all the lines. In most cases, the fit is either the same or slightly better at the wings as can be see in Figure 3.11. However, this correction has no significant effect on the full width at 10%. Due to this insignificant difference, only the values from the Gaussian fits are further considered in this work.

The EW and Hα[10%] methods are generally consistent in the classification of sources. Only for three objects (#65, 80, 81) do the two methods give discrepant results.

3.7.3 Mass Accretion Rate

The Hα[10%] value can not only be used as an indicator of accretion, but also allows a quantitative estimate of the mass accretion rate. Natta et al. (2004) derived a correlation between Hα[10%] and mass accretion rate $\dot{M}_{ac}$ (derived from veiling and Hα profile model fittings):

$$\log \dot{M}_{ac} = -12.89(\pm 0.3) + 9.7(\pm 0.7) \cdot 10^{-3} \mathrm{H}\alpha[10\%]$$

where $\dot{M}_{ac}$ is in M$_\odot$ yr^{-1} and Hα[10%] in km s^{-1}. The relation derived by Natta et al. (2004) was only calibrated for $-11 < \log \dot{M} < -6$. The cut-off of 200 km s^{-1} agrees with a cut-off of $10^{-10.95}$ M$_\odot$ yr^{-1} for $\dot{M}$. With this relation, mass accretion rates can be calculated for the objects in this sample with Hα in emission (see Table 3.4). In Figure 3.12 the distribution of the mass accretion rates is shown. Typical uncertainties are an order of magnitude. Most of the accreters have mass accretion rates that are consistent with the typical range for classical T Tauri stars.

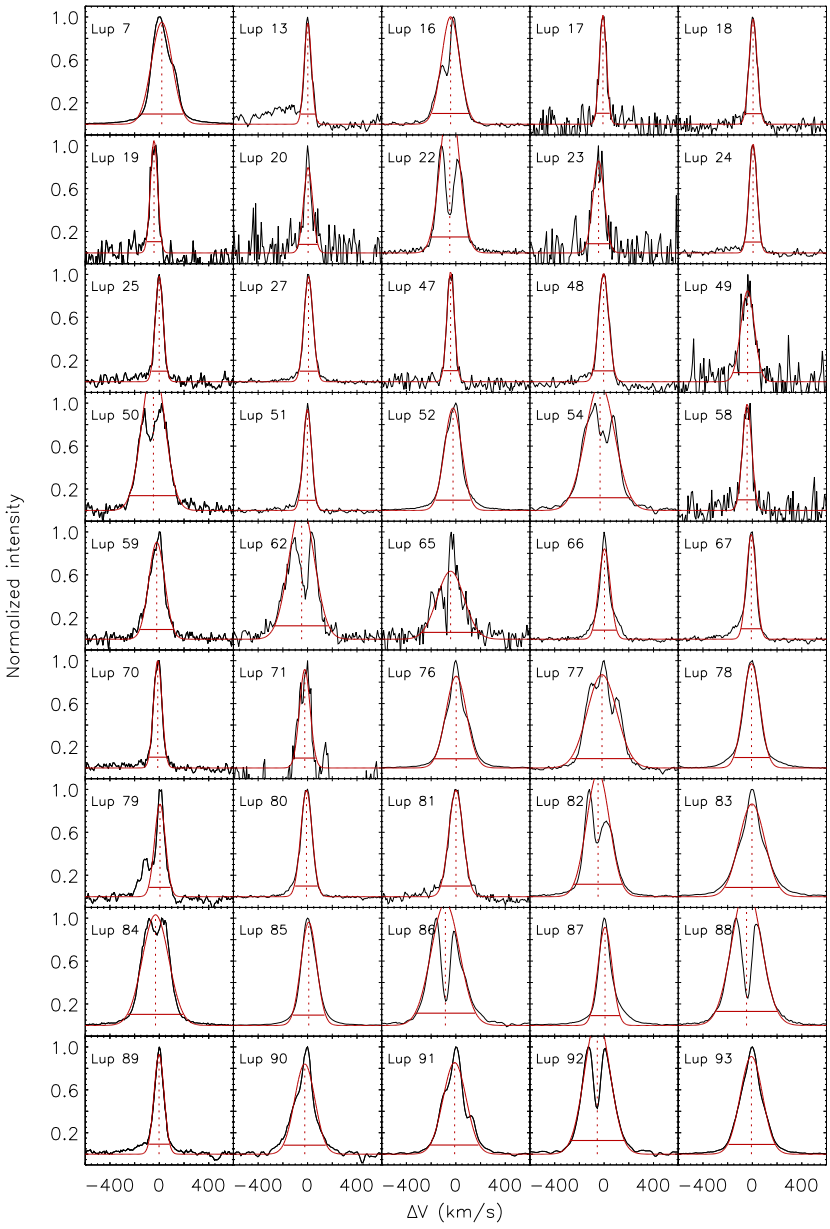

Figure 3.10 – Continuum subtracted, normalized profiles of the Hα emission lines (black line) overplotted with a Gaussian fit (gray solid line). The red dotted line marks the centre of the Gaussian fit and the horizontal gray line marks the width at 10% intensity.

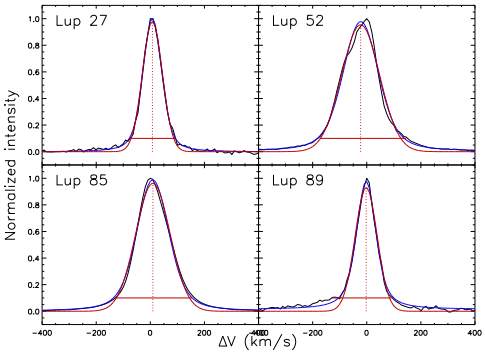

Figure 3.11 – Sample of continuum subtracted, normalized profiles of the Hα emission lines overplotted with a Gaussian fit (light gray solid line) and a Voigt fit (dark gray solid line). The red dotted line marks the center of the Gaussian fit.

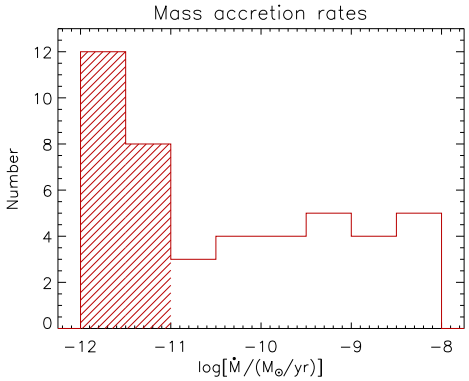

Figure 3.12 – Histogram of the mass accretion rates derived from the Hα[10%] value. The shaded area are objects out of the range for which the relationship of Natta et al. (2004) was calibrated. Those objects are generally classified as non-accreters.

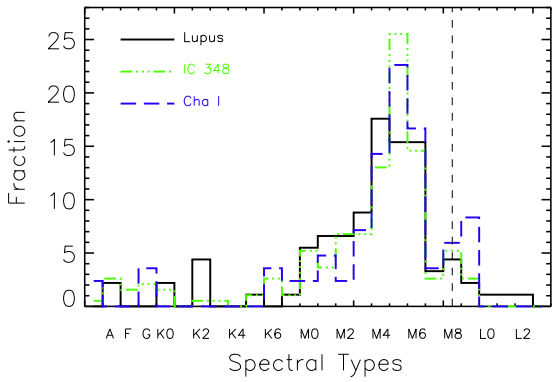

Figure 3.13 – Distribution of spectral types in Lupus (black solid line), IC 348 (light gray dot-dashed line) and Chamaeleon I (dark gray dashed line).

3.8 Discussion

Our work can be added to some of the objects classified as young stars by Merín et al. (2008) that have previously been spectrally classified in the literature in different studies (López Martí et al. 2005; Allers et al. 2006; Allen et al. 2007; Merín et al. 2007; Comerón 2008). This amounts to 91 of the 159 IR excess sources in the sample of Merín et al. (2008) to have known spectral types. This fairly complete sample can be compared to other nearby star-forming regions with equally complete stellar characterization.

Luhman et al. (2003) studied the young cluster IC348. Spectral types are determined with low-resolution optical spectroscopy for 169 objects. Similarly, Luhman (2007) determined spectral types for the 85 targets in the star forming region Chamaeleon I. Figure 3.13 shows the distribution of spectral types in Lupus (this work + literature), in IC 348 and Chamaeleon I. The vertical dashed line shows the completeness of the IC 348 and Cha I samples, which is comparable to the limit achieved by Merín et al. (2008). It can be seen that the three regions show very similar distributions of stellar types, from which is inferred that the IMF of Lupus is very similar to those of IC 348 and Cha I.

It is important to note that the sample of Merín et al. (2008) is selected on the basis of IR excess and it is, by definition, biased against young stars without disks (i.e. no IR excess). A similar study characterizing the young stellar population without disks in Lupus is still lacking.

3.9 Conclusions

We have presented a spectroscopic survey at optical wavelengths designed to determine spectral types and confirm the pre-main sequence nature of a sample of young

stellar objects in the Lupus Clouds found in the *Spitzer* c2d survey.

- Spectral types were determined for 54 stars belonging to Lupus I, III or IV. The sample consists mostly of M-type stars (90%), but also a few K-type stars. No early type object was found in this sample. The distribution of spectral types peaks at M4–M6. The distribution of spectral types is very similar to that of well studied star-forming regions like IC 348 and Chamaeleon I.
- The objects were placed in a H-R diagram after effective temperatures and luminosities were derived. Comparison with theoretical isochrones and mass tracks from models of Baraffe et al. (1998) and Siess et al. (2000) yield individual ages and masses for the objects. 10 objects are too luminous to belong to the clouds, while 3 objects are too faint. The very faint objects could still belong to the clouds by having a remnant envelope or an edge-on disk dimming some of the stellar luminosity.
- The theoretical models by Baraffe et al. (1998) and Siess et al. (2000) imply a population of YSOs concentrated in the age range between 1 and 5 Myr. The mean age is found to be 3.6 and 4.4 Myr with the Baraffe et al. (1998) and Siess et al. (2000) tracks, respectively. Individual masses range from 0.1 to 1.0 $M_\odot$, with mean values of 0.3 $M_\odot$ for both models.
- About half of the sample shows the Hα line in emission, an important indicator of accretion. This relationship was explored in two different ways: the equivalent width of Hα, and its full width at 10% of peak intensity. This confirms 25 objects (or 56% of the YSO sample) to be actively accreting objects classified as classical T Tauri stars. The quantitative estimate of the mass accretion rate $\dot{M}_{\rm ac}$ based on the full width of Hα at 10% of the peak intensity yields a broad distribution of values ($\sim 10^{-11} - 10^{-8}$ $M_\odot {\rm yr}^{-1}$), typical of T Tauri stars.

References

Allard, F., Hauschildt, P. H., Alexander, D. R., Ferguson, J. W., & Tamanai, A. 2000, From Giant Planets to Cool Stars, 212, 127

Allen, P. R., Luhman, K. L., Myers, P. C., Megeath, S. T., Allen, L. E., Hartmann, L., & Fazio, G. G. 2007, ApJ, 655, 1095

Allers, K. N., Kessler-Silacci, J. E., Cieza, L. A., & Jaffe, D. T. 2006, ApJ, 644, 364

Baraffe, I., Chabrier, G., Allard, F., & Hauschildt, P. H. 1998, A&A, 337, 403

Baraffe, I., Chabrier, G., Allard, F., & Hauschildt, P. 2001, From Darkness to Light: Origin and Evolution of Young Stellar Clusters, 243, 571

Comerón, F. 2008, Handbook of Star Forming Regions, Volume II, 295

Comerón, F., Spezzi, L., & López Martí, B. 2009, A&A, 500, 1045

Evans, N. J., II, et al. 2003, PASP, 115, 965

Evans, N. J., et al. 2007, Final Delivery of Data from the c2d Legacy Project: IRAC and MIPS (Pasadena: SSC)[2]

Evans, N. J., et al. 2009, ApJS, 181, 321

Harvey, P. M., et al. 2007, ApJ, 663, 1139

[2]http://ssc.spitzer.caltech.edu/spitzermission/observingprograms/legacy/c2dhistory.html

Harvey, P., Merín, B., Huard, T. L., Rebull, L. M., Chapman, N., Evans, N. J., II, & Myers, P. C. 2007, ApJ, 663, 1149
Hauschildt, P. H., Allard, F., Ferguson, J., Baron, E., & Alexander, D. R. 1999, ApJ, 525, 871
Hughes, J., Hartigan, P., Krautter, J., & Kelemen, J. 1994, AJ, 108, 1071
Jayawardhana, R., Mohanty, S., & Basri, G. 2003, ApJ, 592, 282
Kenyon, S. J., & Hartmann, L. 1995, ApJS, 101, 117
López Martí, B., Eislöffel, J., & Mundt, R. 2005, A&A, 440, 139
Luhman, K. L., Stauffer, J. R., Muench, A. A., Rieke, G. H., Lada, E. A., Bouvier, J., & Lada, C. J. 2003, ApJ, 593, 1093
Luhman, K. L. 2007, ApJS, 173, 104
Merín, B., et al. 2007, ApJ, 661, 361
Merín, B., et al. 2008, ApJS, 177, 551
Merín, B., et al. 2010, ApJ, 718, 1200
Montes, D. 1998, Ap&SS, 263, 275
Natta, A., Testi, L., Muzerolle, J., Randich, S., Comerón, F., & Persi, P. 2004, A&A, 424, 603
Oliveira, I., et al. 2009, ApJ, 691, 672
Siess, L., Dufour, E., & Forestini, M. 2000, A&A, 358, 593
Tothill, N. F. H., et al. 2009, ApJS, 185, 98
Wang, H., & Henning, T. 2009, AJ, 138, 1072
Weingartner, J. C., & Draine, B. T. 2001, ApJ, 548, 296
White, R. J., & Basri, G. 2003, ApJ, 582, 1109

Table 3.1 – ID, name, cloud, position, observing dates and exposure times of the objects.

ID	Name	Cloud	RA (deg)	Dec (deg)	Observing Date	t_{exp} (s)	M[1]
1	2MASSJ16075475-3915446	Lupus III	16 : 07 : 54.72	−39 : 15 : 44.27	2008-02-21	630.0	U
2	2MASSJ16080175-3912316	Lupus III	16 : 08 : 01.68	−39 : 12 : 31.31	2008-02-21	630.0	U
3	2MASSJ16080618-3912225	Lupus III	16 : 08 : 06.24	−39 : 12 : 22.32	2008-02-21	630.0	S
4	2MASSJ16081497-3857145	Lupus III	16 : 08 : 14.88	−38 : 57 : 14.77	2008-02-21	630.0	U
5	2MASSJ16084747-3905087	Lupus III	16 : 08 : 47.52	−39 : 05 : 08.17	2008-02-21	630.0	U
6	2MASSJ16085373-3914367	Lupus III	16 : 08 : 53.76	−39 : 14 : 36.96	2008-02-21	630.0	U
7	2MASSJ16085529-3848481	Lupus III	16 : 08 : 55.20	−38 : 48 : 48.24	2008-02-22	1000.0	X
8	2MASSJ16085953-3856275	Lupus III	16 : 08 : 59.52	−38 : 56 : 27.96	2008-02-21	630.0	U
9	AKC2006-17	Lupus I	15 : 39 : 27.36	−34 : 48 : 43.56	2008-02-23	800.0	U
10	IRACJ16083010-3922592	Lupus III	16 : 08 : 30.00	−39 : 22 : 59.15	2008-02-26	1000.0	U
11	IRACJ16084679-3902074	Lupus III	16 : 08 : 46.80	−39 : 02 : 07.44	2008-02-21	630.0	U
12	IRACJ16093418-3915127	Lupus III	16 : 09 : 34.08	−39 : 15 : 12.61	2008-02-26	1000.0	U
13	IRAS15567-4141	Lupus IV	16 : 00 : 07.44	−41 : 49 : 48.72	2008-02-21	550.0	X
14	IRAS15589-4132	Lupus IV	16 : 02 : 21.60	−41 : 40 : 53.76	2008-02-24	1000.0	W
16	Lup604s	Lupus III	16 : 08 : 00.24	−39 : 02 : 58.93	2008-02-21	630.0	X
17	Lup607	Lupus III	16 : 08 : 28.08	−39 : 13 : 09.83	2008-02-21	630.0	S
18	Lup608s	Lupus III	16 : 09 : 08.40	−39 : 03 : 42.84	2008-02-21	630.0	S
19	Lup617	Lupus III	16 : 08 : 48.24	−39 : 09 : 19.44	2008-02-21	630.0	S
20	Lup650	Lupus III	16 : 09 : 49.92	−38 : 49 : 02.65	2008-02-22	1000.0	S
21	Lup654	Lupus III	16 : 07 : 23.52	−39 : 05 : 09.97	2008-02-21	630.0	N
22	Lup706	Lupus III	16 : 08 : 37.44	−39 : 23 : 11.03	2008-02-26	1000.0	N
23	Lup710	Lupus III	16 : 09 : 17.04	−39 : 27 : 09.73	2008-02-23	1000.0	S
24	Lup714	Lupus III	16 : 07 : 58.80	−39 : 24 : 34.91	2008-02-26	1000.0	X
25	Lup802s	Lupus III	16 : 11 : 51.12	−38 : 51 : 05.03	2008-02-26	1000.0	X
26	Lup810s	Lupus III	16 : 09 : 54.48	−39 : 12 : 03.24	2008-02-22	1000.0	S
27	Lup818s	Lupus III	16 : 09 : 56.40	−38 : 59 : 51.00	2008-02-22	1000.0	X
28	Lupus3MMS	Lupus III	16 : 09 : 18.00	−39 : 04 : 53.40	2008-02-24	10.0	N
					2008-02-26	1000.0	
29	NTO2000-0526.9-5630	Lupus III	16 : 08 : 28.08	−39 : 04 : 24.61	2008-02-21	630.0	U
30	NTO2000-0532.1-5616	Lupus III	16 : 08 : 53.52	−39 : 04 : 09.11	2008-02-21	630.0	U
31	NTO2000-0536.7-5943	Lupus III	16 : 08 : 58.32	−39 : 07 : 35.40	2008-02-24	1000.0	N
32	NTO2000-0536.7-5956	Lupus III	16 : 08 : 58.32	−39 : 07 : 49.45	2008-02-24	10.0	N
					2008-02-26	1000.0	
33	NTO2000-0537.4-5653	Lupus III	16 : 08 : 59.04	−39 : 04 : 45.84	2008-02-21	630.0	U
34	NTO2000-0540.9-5757	Lupus III	16 : 09 : 02.40	−39 : 05 : 49.20	2008-02-21	630.0	N
35	NTO2000-0546.4-5934	Lupus III	16 : 09 : 07.92	−39 : 07 : 26.76	2008-02-24	10.0	N
					2008-02-26	1000.0	
36	NTO2000-0554.9-5651	Lupus III	16 : 09 : 16.32	−39 : 04 : 43.68	2008-02-24	1000.0	N
37	NTO2000-0558.8-5610	Lupus III	16 : 09 : 20.40	−39 : 04 : 01.56	2008-02-24	10.0	N
					2008-02-26	1000.0	
38	NTO2000-0601.7-5616	Lupus III	16 : 09 : 23.04	−39 : 04 : 07.32	2008-02-24	10.0	N
					2008-02-26	1000.0	
39	NTO2000-0605.1-5606	Lupus III	16 : 09 : 26.64	−39 : 03 : 57.61	2008-02-26	1000.0	U
40	NTO2000-0605.6-5437	Lupus III	16 : 09 : 27.12	−39 : 02 : 28.32	2008-02-21	630.0	U
41	NTO2000-0614.0-5414	Lupus III	16 : 09 : 35.52	−39 : 02 : 05.64	2008-02-21	630.0	U
42	NTO2000-0615.6-5616	Lupus III	16 : 09 : 37.20	−39 : 04 : 06.96	2008-02-24	1000.0	U
43	NTO2000-0615.6-5953	Lupus III	16 : 09 : 37.20	−39 : 07 : 44.76	2008-02-24	1000.0	U
44	NTO2000-0615.8-5734	Lupus III	16 : 09 : 37.44	−39 : 05 : 25.80	2008-02-24	1000.0	U
45	NTO2000-0617.7-5641	Lupus III	16 : 09 : 39.36	−39 : 04 : 31.80	2008-02-24	1000.0	U
46	NTO2000-0619.6-5414	Lupus III	16 : 09 : 41.04	−39 : 02 : 05.64	2008-02-21	630.0	U
47	Par-Lup3-1	Lupus III	16 : 08 : 16.08	−39 : 03 : 03.97	2008-02-21	630.0	S
48	Par-Lup3-2	Lupus III	16 : 08 : 35.76	−39 : 03 : 47.53	2008-02-21	630.0	X
49	Par-Lup3-3	Lupus III	16 : 08 : 49.44	−39 : 05 : 39.12	2008-02-21	630.0	N
50	Par-Lup3-4	Lupus III	16 : 08 : 51.36	−39 : 05 : 30.13	2008-02-21	630.0	N
51	SST-Lup3-1	Lupus III	16 : 11 : 59.76	−38 : 23 : 38.40	2008-02-25	1000.0	X
52	SSTc2dJ155925.2-423507	Lupus IV	15 : 59 : 25.20	−42 : 35 : 07.08	2008-02-26	1000.0	S
53	SSTc2dJ160000.6-422158	Lupus IV	16 : 00 : 00.48	−42 : 21 : 57.23	2008-02-26	1000.0	W
54	SSTc2dJ160002.4-422216	Lupus IV	16 : 00 : 02.40	−42 : 22 : 14.88	2008-02-26	1000.0	X
55	SSTc2dJ160111.6-413730	Lupus IV	16 : 01 : 11.52	−41 : 37 : 30.00	2008-02-21	550.0	X
56	SSTc2dJ160143.3-413606	Lupus IV	16 : 01 : 43.20	−41 : 36 : 05.76	2008-02-21	550.0	X
57	SSTc2dJ160229.9-415111	Lupus IV	16 : 02 : 30.00	−41 : 51 : 10.80	2008-02-24	1000.0	S
58	SSTc2dJ160703.9-391112	Lupus III	16 : 07 : 03.84	−39 : 11 : 11.40	2008-02-21	630.0	S
59	SSTc2dJ160708.6-391407	Lupus III	16 : 07 : 08.64	−39 : 14 : 07.44	2008-02-21	630.0	N
60	SSTc2dJ160755.3-390718	Lupus III	16 : 07 : 55.20	−39 : 07 : 17.39	2008-02-21	630.0	S
61	SSTc2dJ160803.0-385229	Lupus III	16 : 08 : 03.12	−38 : 52 : 29.64	2008-02-24	1000.0	X
62	SSTc2dJ160901.4-392512	Lupus III	16 : 09 : 01.44	−39 : 25 : 11.99	2008-02-23	1000.0	S
63	SSTc2dJ160934.1-391342	Lupus III	16 : 09 : 34.08	−39 : 13 : 42.24	2008-02-21	630.0	S
64	SSTc2dJ161000.1-385401	Lupus III	16 : 10 : 00.00	−38 : 54 : 00.36	2008-02-22	1000.0	X
65	SSTc2dJ161013.1-384617	Lupus III	16 : 10 : 12.96	−38 : 46 : 16.31	2008-02-22	1000.0	S
66	SSTc2dJ161019.8-383607	Lupus III	16 : 10 : 19.92	−38 : 36 : 06.48	2008-02-23	1000.0	X

ID	Name	Cloud	RA (deg)	Dec (deg)	Observing Date	t_{exp} (s)	M[1]
67	SSTc2dJ161029.6-392215	Lupus III	16 : 10 : 29.52	−39 : 22 : 14.52	2008-02-23	1000.0	X
68	SSTc2dJ161034.5-381450	Lupus III	16 : 10 : 34.56	−38 : 14 : 50.28	2008-02-25	1000.0	X
69	SSTc2dJ161131.9-381110	Lupus III	16 : 11 : 31.92	−38 : 11 : 09.96	2008-02-25	1000.0	S
70	SSTc2dJ161144.9-383245	Lupus III	16 : 11 : 44.88	−38 : 32 : 44.88	2008-02-23	1000.0	X
71	SSTc2dJ161148.7-381758	Lupus III	16 : 11 : 48.72	−38 : 17 : 57.84	2008-02-25	1000.0	S
72	SSTc2dJ161204.5-380959	Lupus III	16 : 12 : 04.56	−38 : 09 : 58.69	2008-02-25	1000.0	U
73	SSTc2dJ161211.2-383220	Lupus III	16 : 12 : 11.28	−38 : 32 : 20.03	2008-02-22	1000.0	U
74	SSTc2dJ161219.6-383742	Lupus III	16 : 12 : 19.68	−38 : 37 : 41.88	2008-02-22	1000.0	S
75	SSTc2dJ161251.7-384216	Lupus III	16 : 12 : 51.60	−38 : 42 : 15.84	2008-02-22	1000.0	S
76	Sz100	Lupus III	16 : 08 : 25.68	−39 : 06 : 01.08	2008-02-21	300.0	X
					2008-02-23	200.0	
					2008-02-26	200.0	
77	Sz101	Lupus III	16 : 08 : 28.32	−39 : 05 : 31.92	2008-02-21	630.0	X
78	Sz102	Lupus III	16 : 08 : 29.76	−39 : 03 : 10.81	2008-02-21	630.0	S
79	Sz103	Lupus III	16 : 08 : 30.24	−39 : 06 : 10.80	2008-02-21	630.0	X
80	Sz104	Lupus III	16 : 08 : 30.72	−39 : 05 : 48.49	2008-02-21	630.0	X
81	Sz107	Lupus III	16 : 08 : 41.76	−39 : 01 : 36.84	2008-02-21	630.0	S
82	Sz108B	Lupus III	16 : 08 : 42.96	−39 : 06 : 14.40	2008-02-21	630.0	X
					2008-02-23	200.0	
					2008-02-26	200.0	
83	Sz110	Lupus III	16 : 08 : 51.60	−39 : 03 : 17.64	2008-02-21	300.0	S
					2008-02-23	200.0	
					2008-02-26	200.0	
84	Sz113	Lupus III	16 : 08 : 57.84	−39 : 02 : 22.56	2008-02-21	630.0	X
85	Sz114	Lupus III	16 : 09 : 01.92	−39 : 05 : 12.12	2008-02-21	300.0	X
					2008-02-23	200.0	
					2008-02-26	200.0	
86	Sz118	Lupus III	16 : 09 : 48.72	−39 : 11 : 16.80	2008-02-22	1000.0	S
87	Sz130	Lupus IV	16 : 00 : 30.96	−41 : 43 : 36.83	2008-02-21	550.0	X
88	Sz133	Lupus IV	16 : 03 : 29.52	−41 : 40 : 02.28	2008-02-24	1000.0	S
89	Sz94	Lupus III	16 : 07 : 49.68	−39 : 04 : 28.56	2008-02-21	630.0	S
90	Sz96	Lupus III	16 : 08 : 12.48	−39 : 08 : 33.01	2008-02-21	630.0	S
91	Sz97	Lupus III	16 : 08 : 21.84	−39 : 04 : 21.36	2008-02-21	630.0	X
					2008-02-23	200.0	
					2008-02-26	200.0	
92	Sz98	Lupus III	16 : 08 : 22.56	−39 : 04 : 45.84	2008-02-21	300.0	S
					2008-02-23	200.0	
					2008-02-26	200.0	
93	Sz99	Lupus III	16 : 08 : 24.00	−39 : 05 : 49.20	2008-02-21	630.0	X
					2008-02-23	200.0	
					2008-02-26	200.0	

[1] G means good spectra, U non-detections, F featureless spectra, and O not useful spectra. See Section 3.4.3 for more details.

Table 3.2 – Spectral types, visual extinction (A_V), normalization bands and the spectral index, calculated between the 2MASS K-band (2 μm) and the MIPS1 band (24 μm), for the classifiable objects. Objects for which SEDs could not be produced do not have all values.

ID	SpT	Range	A_V (mag)	Band	$\alpha_{2-24\mu m}$	Class
3	M6.5	M4 - M8.5	5.30	J	−1.91	III
7	M3	M2 - M4	2.50	Z	−1.25	II
13	M6.5	M4 - M8.5	2.00	J	−1.54	II
16	M5.5	M4 - M6	1.20	Z	−1.21	II
17	M5.5	M4 - M6	0.00	Z		
18	M5.5	M4 - M8.5				
19	M6	M4 - M8.5				
20	M3.5	M2 - M4				
23	M4.5	M3 - M6				
24	M6	M4 - M8.5				
25	M5.5	M4 - M6				
26	K0	K0 - K2				
27	M6	M4 - M8.5	1.40	Z	−1.01	II
47	M5.5	M4 - M6				
48	M5	M4 - M6				
51	M6	M4 - M8.5	1.80	J	−1.08	II
52	M4.5	M3 - M6				
54	M3.5	M2 - M4				
55	M8.5	M6 - M9.5	0.00	J	−2.30	III
56	M6	M4 - M8.5	1.20	J	−2.36	III
57	M7	M4 - M9	2.60	J	−2.27	III
58	M5.5	M3 - M6	2.20	Z	−0.17	II
60	M9	M8.5 - M9.5	8.00	Z	−2.16	III
61	M5.5	M4 - M6	2.00	Z	−2.39	III
62	M3.5	M2 - M4	0.60	J	−1.10	II
63	M7.5	M6 - M9	3.40	Z	−2.49	III
64	M6.5	M6 - M8.5	2.80	J	−1.82	III
65	M4	M3 - M6	0.70	Z	−0.21	II
66	M6	M4 - M8.5	0.40	J	−1.18	II
67	M5.5	M3 - M6	0.00	J	−0.93	II
68	M6.5	M6 - M8.5	2.90	J	−2.31	III
69	M2.5	M0.5 - M4	1.90	J	−2.30	III
70	M6.5	M4 - M8.5	0.00	J	−1.99	III
71	K2	K0 - K7	1.60	J	−0.60	II
74	M8	M6 - M8.5	1.60	J	−2.34	III
75	M8.5	M6 - M9.5	1.00	J	−2.15	III
76	M4.5	M3 - M6	1.20	Z	−0.80	II
77	M4.5	M3 - M6	0.70	Z	−1.68	III
78	K2	K0 - K7	2.50	J	0.59	I
79	M4.5	M3 - M6	1.00	Z	−0.86	II
80	M5.5	M3 - M6	0.70	Z	−0.91	II
81	M6.5	M4 - M8.5	0.00	Z	−1.64	III
82	M5.5	M3 - M6	0.80	Z		
83	M3	M0.5 - M4	0.20	J	−0.71	II
84	M1.5	K7 - M2	2.40	Z	−0.67	II
85	M4	M3 - M6	1.30	Z	−0.62	II
86	K7	K2 - M0	2.60	J	−0.90	II
87	M2	M0.5 - M4	0.60	J	−0.94	II
88	K2	K0 - K7				
89	M4.5	M3 - M6				
90	M2	M0 - M3	1.43	J	−0.91	II
91	M4.5	M3 - M6	0.30	Z	−1.24	II
92	K5	K2 - M0.5	2.50	J	−0.64	II
93	M4	M3 - M6	0.40	J	−1.12	II

Note: Sources without ages and masses do not follow the evolutionary tracks.

Table 3.3 – Effective temperature $T_{\rm eff}$, stellar and disk luminosity, L_* and $L_{\rm disk}$, age and mass for Baraffe et al. (1998 - 2001) and Siess et al. (2000).

ID	$T_{\rm eff}$ (K)	L_* ($L_\odot$)	$L_{\rm disk}$ ($L_\odot$)	Age_B (Myr)	$Mass_B$ ($M_\odot$)	Age_S (Myr)	$Mass_S$ ($M_\odot$)
3	$2935.0^{+335.0}_{-380.0}$	$2.09^{+0.80}_{-0.61}$	$0.61^{+0.45}_{-0.31}$				
7	$3415.0^{+145.0}_{-145.0}$	$0.06^{+0.03}_{-0.02}$	$0.01^{+0.01}_{-0.01}$	$13.64^{+14.82}_{-7.21}$	$0.35^{+0.15}_{-0.12}$	$9.90^{+6.37}_{-3.46}$	$0.27^{+0.07}_{-0.06}$
13	$2935.0^{+335.0}_{-380.0}$	$2.74^{+1.28}_{-0.94}$	$1.93^{+1.05}_{-0.74}$				
16	$3057.5^{+212.5}_{-67.5}$	$0.09^{+0.05}_{-0.03}$	$0.02^{+0.02}_{-0.02}$	$1.17^{+2.79}_{-0.78}$	$0.12^{+0.13}_{-0.02}$	$3.85^{+0.96}_{-3.85}$	$0.14^{+0.08}_{-0.02}$
17	$3057.5^{+212.5}_{-67.5}$	$0.01^{+0.00}_{-0.00}$	$0.00^{+0.01}_{-0.00}$	$12.75^{+42.27}_{-4.13}$	$0.09^{+0.09}_{-0.02}$	$16.25^{+48.83}_{-7.41}$	$0.09^{+0.09}_{-0.02}$
27	$2990.0^{+280.0}_{-435.0}$	$0.04^{+0.02}_{-0.02}$	$0.01^{+0.01}_{-0.01}$	$1.87^{+7.16}_{-1.87}$	$0.09^{+0.13}_{-0.09}$	$4.43^{+4.99}_{-2.82}$	$0.09^{+0.10}_{-0.09}$
51	$2990.0^{+280.0}_{-435.0}$	$0.12^{+0.04}_{-0.03}$	$0.01^{+0.02}_{-0.01}$	$0.19^{+2.79}_{-0.19}$	$0.11^{+0.15}_{-0.11}$	$3.62^{+0.59}_{-0.59}$	$0.17^{+0.06}_{-0.06}$
55	$2555.0^{+435.0}_{-255.0}$	$0.17^{+0.08}_{-0.06}$	$0.05^{+0.05}_{-0.02}$				
56	$2990.0^{+280.0}_{-435.0}$	$0.37^{+0.17}_{-0.13}$	$0.06^{+0.08}_{-0.04}$	$0.00^{+0.57}_{-0.00}$	$0.18^{+0.12}_{-0.18}$	$1.81^{+-1.81}_{-1.81}$	$0.26^{+-0.26}_{-0.26}$
57	$2880.0^{+390.0}_{-480.0}$	$0.15^{+0.07}_{-0.05}$	$0.03^{+0.03}_{-0.02}$	$0.00^{+2.44}_{-0.00}$	$0.06^{+5.02}_{-0.00}$	$3.40^{+-3.40}_{-3.40}$	$0.24^{+-0.24}_{-0.24}$
58	$3057.5^{+357.5}_{-67.5}$	$0.01^{+0.01}_{-0.00}$	$0.02^{+0.01}_{-0.01}$	$9.83^{+131.97}_{-2.07}$	$0.09^{+0.20}_{-0.02}$	$13.83^{+101.47}_{-5.94}$	$0.09^{+0.16}_{-0.02}$
60	$2400.0^{+155.0}_{-100.0}$	$1.94^{+0.95}_{-0.66}$	$0.80^{+0.61}_{-0.40}$				
61	$3057.5^{+212.5}_{-67.5}$	$1.22^{+0.60}_{-0.42}$	$0.19^{+0.33}_{-0.19}$				
62	$3342.5^{+217.5}_{-72.5}$	$0.16^{+0.06}_{-0.05}$	$0.06^{+0.03}_{-0.03}$	$2.86^{+5.43}_{-0.69}$	$0.31^{+0.20}_{-0.05}$	$3.49^{+1.67}_{-0.67}$	$0.27^{+0.09}_{-0.03}$
63	$2795.0^{+195.0}_{-395.0}$	$2.93^{+1.43}_{-1.00}$	$1.14^{+0.94}_{-0.61}$				
64	$2935.0^{+55.0}_{-380.0}$	$1.56^{+0.60}_{-0.45}$	$0.45^{+0.34}_{-0.23}$				
65	$3270.0^{+145.0}_{-280.0}$	$0.00^{+0.00}_{-0.00}$	$0.00^{+0.01}_{-0.00}$				
66	$2990.0^{+280.0}_{-435.0}$	$0.03^{+0.01}_{-0.01}$	$0.00^{+0.01}_{-0.00}$	$3.07^{+12.27}_{-3.07}$	$0.09^{+0.12}_{-0.09}$	$5.02^{+9.65}_{-2.91}$	$0.08^{+0.10}_{-0.08}$
67	$3057.5^{+357.5}_{-67.5}$	$0.09^{+0.04}_{-0.03}$	$0.02^{+0.02}_{-0.01}$	$1.17^{+7.21}_{-0.78}$	$0.12^{+0.24}_{-0.02}$	$3.85^{+2.80}_{-3.85}$	$0.14^{+0.14}_{-0.02}$
68	$2935.0^{+55.0}_{-380.0}$	$7.12^{+2.72}_{-2.07}$	$0.99^{+1.27}_{-0.82}$				
69	$3487.5^{+290.0}_{-217.5}$	$0.13^{+0.05}_{-0.04}$	$0.02^{+0.02}_{-0.02}$	$7.98^{+19.47}_{-5.19}$	$0.44^{+0.26}_{-0.18}$	$5.74^{+8.90}_{-1.79}$	$0.33^{+0.19}_{-0.09}$
70	$2935.0^{+335.0}_{-380.0}$	$0.06^{+0.02}_{-0.02}$	$0.00^{+0.01}_{-0.00}$	$0.44^{+7.07}_{-0.44}$	$0.08^{+0.15}_{-0.08}$	$3.57^{+4.02}_{-2.32}$	$0.08^{+0.12}_{-0.08}$
71	$4900.0^{+350.0}_{-840.0}$	$0.04^{+0.02}_{-0.01}$	$0.02^{+0.01}_{-0.01}$				
74	$2710.0^{+280.0}_{-155.0}$	$2.44^{+0.93}_{-0.71}$	$0.38^{+0.43}_{-0.29}$				
75	$2555.0^{+435.0}_{-255.0}$	$2.30^{+0.88}_{-0.67}$	$0.57^{+0.47}_{-0.31}$				
76	$3197.5^{+217.5}_{-207.5}$	$0.27^{+0.13}_{-0.09}$	$0.10^{+0.09}_{-0.05}$	$0.53^{+1.73}_{-0.53}$	$0.20^{+0.20}_{-0.04}$	$1.94^{+0.75}_{-1.94}$	$0.23^{+0.08}_{-0.02}$
77	$3197.5^{+217.5}_{-207.5}$	$0.41^{+0.20}_{-0.14}$	$0.06^{+0.10}_{-0.06}$	$0.15^{+1.25}_{-0.15}$	$0.19^{+0.26}_{-0.01}$	$0.82^{+1.34}_{-0.82}$	$0.25^{+0.07}_{-0.02}$
78	$4900.0^{+350.0}_{-840.0}$	$0.03^{+0.01}_{-0.01}$	$0.13^{+0.04}_{-0.03}$				
79	$3197.5^{+217.5}_{-207.5}$	$0.20^{+0.10}_{-0.07}$	$0.06^{+0.06}_{-0.04}$	$0.99^{+1.86}_{-0.98}$	$0.20^{+0.18}_{-0.07}$	$2.48^{+0.67}_{-2.48}$	$0.22^{+0.09}_{-0.04}$
80	$3057.5^{+357.5}_{-67.5}$	$0.13^{+0.06}_{-0.04}$	$0.04^{+0.04}_{-0.02}$	$0.64^{+5.03}_{-0.51}$	$0.13^{+0.24}_{-0.01}$	$2.82^{+1.96}_{-2.82}$	$0.15^{+0.14}_{-0.02}$
81	$2935.0^{+335.0}_{-380.0}$	$0.15^{+0.07}_{-0.05}$	$0.01^{+0.04}_{-0.01}$	$0.00^{+2.36}_{-0.00}$	$0.10^{+0.16}_{-0.10}$	$3.28^{+-3.28}_{-3.28}$	$0.24^{+-0.24}_{-0.24}$
82	$3057.5^{+357.5}_{-67.5}$	$0.09^{+0.05}_{-0.03}$	$0.03^{+0.03}_{-0.02}$	$1.18^{+7.23}_{-0.79}$	$0.12^{+0.24}_{-0.02}$	$3.86^{+2.82}_{-3.86}$	$0.14^{+0.14}_{-0.02}$
83	$3415.0^{+362.5}_{-145.0}$	$0.26^{+0.10}_{-0.08}$	$0.09^{+0.06}_{-0.04}$	$2.35^{+7.10}_{-1.20}$	$0.40^{+0.38}_{-0.12}$	$2.73^{+2.25}_{-0.38}$	$0.31^{+0.20}_{-0.06}$
84	$3632.5^{+427.5}_{-72.5}$	$0.11^{+0.05}_{-0.04}$	$0.04^{+0.03}_{-0.03}$	$19.64^{+59.62}_{-9.80}$	$0.58^{+0.08}_{-0.08}$	$9.95^{+50.10}_{-3.95}$	$0.40^{+0.24}_{-0.04}$
85	$3270.0^{+145.0}_{-280.0}$	$0.49^{+0.24}_{-0.17}$	$0.22^{+0.16}_{-0.11}$	$0.26^{+0.81}_{-0.26}$	$0.32^{+0.16}_{-0.10}$	$1.12^{+0.96}_{-1.12}$	$0.27^{+0.05}_{-0.01}$
86	$4060.0^{+840.0}_{-210.0}$	$0.92^{+0.35}_{-0.27}$	$0.56^{+0.27}_{-0.21}$	$3.72^{+20.71}_{-1.37}$	$1.16^{+0.04}_{-0.16}$	$2.54^{+13.53}_{-1.09}$	$0.76^{+0.39}_{-0.20}$
87	$3560.0^{+217.5}_{-290.0}$	$0.21^{+0.10}_{-0.07}$	$0.06^{+0.06}_{-0.03}$	$5.77^{+7.30}_{-4.20}$	$0.52^{+0.23}_{-0.25}$	$3.74^{+3.02}_{-1.03}$	$0.37^{+0.14}_{-0.12}$
90	$3560.0^{+290.0}_{-145.0}$	$0.82^{+0.31}_{-0.24}$	$0.27^{+0.19}_{-0.13}$	$0.88^{+1.79}_{-0.56}$	$0.67^{+0.32}_{-0.08}$	$0.81^{+0.94}_{-0.81}$	$0.39^{+0.18}_{-0.06}$
91	$3197.5^{+217.5}_{-207.5}$	$0.18^{+0.09}_{-0.06}$	$0.04^{+0.05}_{-0.03}$	$1.29^{+1.86}_{-1.27}$	$0.21^{+0.16}_{-0.08}$	$2.70^{+1.00}_{-2.70}$	$0.22^{+0.09}_{-0.05}$
92	$4350.0^{+550.0}_{-572.5}$	$2.35^{+0.90}_{-0.68}$	$1.18^{+0.66}_{-0.47}$	$2.42^{+3.02}_{-2.24}$	$1.53^{+0.39}_{-0.45}$	$1.49^{+3.46}_{-1.49}$	$1.12^{+0.54}_{-0.65}$
93	$3270.0^{+145.0}_{-280.0}$	$0.11^{+0.04}_{-0.03}$	$0.03^{+0.02}_{-0.02}$	$3.07^{+3.72}_{-2.85}$	$0.26^{+0.11}_{-0.15}$	$4.34^{+1.22}_{-4.34}$	$0.23^{+0.06}_{-0.10}$

Table 3.4 – Hα line widths and mass accretion rates.

ID	EW[Hα] (Å)	CTTS?	Hα [10%] (km s^{-1})	CTTS?	log $\dot{M}_{\rm ac}$ ($M_\odot$ yr^{-1})	Double peak?
7	201.3	yes	351.0 ± 5.0	yes	-9.5 ± 0.4	
13	4.1		98.0 ± 11.0		-11.9 ± 0.3	
16	27.2	yes	306.0 ± 4.0	yes	-9.9 ± 0.4	yes
17	4.7		94.0 ± 11.5		-12.0 ± 0.3	
18	7.1		116.0 ± 7.5		-11.8 ± 0.3	
19	2.2		100.0 ± 11.0		-11.9 ± 0.3	yes
20	8.2		137.0 ± 16.5		-11.6 ± 0.3	
22	327.3	yes	312.0 ± 4.5	yes	-9.9 ± 0.4	yes
23	5.2		183.0 ± 16.0		-11.1 ± 0.4	yes
24	10.6		115.0 ± 6.0		-11.8 ± 0.3	
25	7.0		112.0 ± 7.0		-11.8 ± 0.3	
27	36.6		137.0 ± 5.5		-11.6 ± 0.3	
47	9.8		104.0 ± 8.0		-11.9 ± 0.3	yes
48	3.4		159.0 ± 7.0		-11.3 ± 0.3	
49	44.7	yes	224.0 ± 19.5	yes	-10.7 ± 0.4	yes
50	147.2	yes	385.0 ± 6.5	yes	-9.2 ± 0.4	yes
51	11.5		125.0 ± 6.0		-11.7 ± 0.3	
52	130.8	yes	289.0 ± 4.0	yes	-10.1 ± 0.4	
54	26.8	yes	501.0 ± 6.0	yes	-8.0 ± 0.5	yes
58	10.7		139.0 ± 11.0		-11.5 ± 0.3	yes
59	255.6	yes	264.0 ± 8.0	yes	-10.3 ± 0.4	
62	22.3	yes	431.0 ± 10.5	yes	-8.7 ± 0.4	yes
65	17.7		463.0 ± 27.5	yes	-8.4 ± 0.5	yes
66	23.6		181.0 ± 6.0		-11.1 ± 0.3	
67	9.4		149.0 ± 6.0		-11.4 ± 0.3	
70	11.9		123.0 ± 6.5		-11.7 ± 0.3	
71	-0.7		167.0 ± 24.0		-11.3 ± 0.4	
76	97.8	yes	348.0 ± 4.5	yes	-9.5 ± 0.4	
77	23.7	yes	504.0 ± 9.0	yes	-8.0 ± 0.5	
78	333.6	yes	283.0 ± 7.0	yes	-10.1 ± 0.4	
79	6.4		171.0 ± 9.5		-11.2 ± 0.3	
80	26.8	yes	182.0 ± 4.5		-11.1 ± 0.3	
81	10.5		236.0 ± 6.0	yes	-10.6 ± 0.3	
82	68.8	yes	389.0 ± 6.0	yes	-9.1 ± 0.4	yes
83	71.8	yes	440.0 ± 5.5	yes	-8.6 ± 0.4	
84	267.2	yes	450.0 ± 6.5	yes	-8.5 ± 0.4	yes
85	139.2	yes	261.0 ± 3.5	yes	-10.4 ± 0.3	
86	41.0	yes	486.0 ± 6.0	yes	-8.2 ± 0.5	yes
87	58.3	yes	229.0 ± 5.0	yes	-10.7 ± 0.3	
88	121.7	yes	498.0 ± 4.0	yes	-8.1 ± 0.5	yes
89	7.5		156.0 ± 6.0		-11.4 ± 0.3	
90	11.4	yes	344.0 ± 6.5	yes	-9.5 ± 0.4	
91	38.7	yes	395.0 ± 6.5	yes	-9.1 ± 0.4	
92	26.4	yes	432.0 ± 4.0	yes	-8.7 ± 0.4	yes
93	117.0	yes	379.0 ± 3.0	yes	-9.2 ± 0.4	